

VividDreamer: Towards High-Fidelity and Efficient Text-to-3D Generation

Zixuan Chen, Ruijie Su, Jiahao Zhu, Lingxiao Yang, *Member, IEEE*, Jian-Huang Lai, *Senior Member, IEEE*, and Xiaohua Xie, *Member, IEEE*

Abstract—Text-to-3D generation aims to create 3D assets from text-to-image diffusion models. However, existing methods face an inherent bottleneck in generation quality because the widely-used objectives such as Score Distillation Sampling (SDS) inappropriately omit U-Net jacobians for swift generation, leading to significant bias compared to the “true” gradient obtained by full denoising sampling. This bias brings inconsistent updating direction, resulting in implausible 3D generation (e.g., color deviation, Janus problem, and semantically inconsistent details). In this work, we propose *Pose-dependent Consistency Distillation Sampling* (PCDS), a novel yet efficient objective for diffusion-based 3D generation tasks. Specifically, *PCDS* builds the *pose-dependent consistency function* within diffusion trajectories, allowing to approximate true gradients through minimal sampling steps (1~3). Compared to SDS, *PCDS* can acquire a more accurate updating direction with the same sampling time (1 sampling step), while enabling few-step (2~3) sampling to trade compute for higher generation quality. For efficient generation, we propose a *coarse-to-fine optimization strategy*, which first utilizes 1-step *PCDS* to create the basic structure of 3D objects, and then gradually increases *PCDS* steps to generate fine-grained details. Extensive experiments demonstrate that our approach outperforms the state-of-the-art in generation quality and training efficiency, conspicuously alleviating the implausible 3D generation issues caused by the deviated updating direction. Moreover, it can be simply applied to many 3D generative applications to yield impressive 3D assets, please see [Project page](#).

Index Terms—Text-to-3D Generation, Diffusion Models, Consistency Models, 3D Gaussian Splatting

I. INTRODUCTION

TEXT-TO-3D generation aims to create 3D objects with words, which used to sound like a tale from the *Arabian Nights* as it relies on the organic combination between efficient 3D representation techniques and powerful generative models. With the emergence of key technologies such as Neural Radiance Fields (NeRF) [1] and text-to-image diffusion models [2], [3], numerous works [4]–[7] quickly sprout up in recent years. These methods generate NeRF-based 3D representation from the 3D priors distilled from the pre-trained diffusion model, making it possible to create imaginative 3D assets in the real

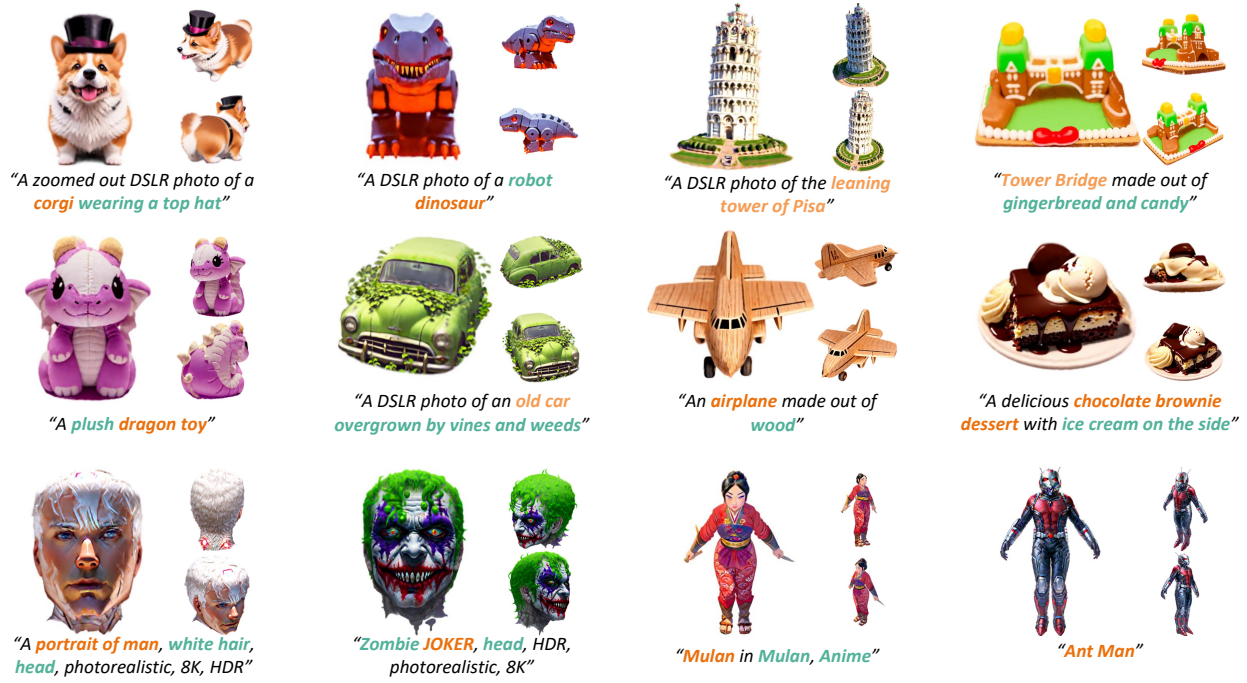
world. To accelerate the training process, current methods [8]–[10] introduce 3D Gaussian Splatting (3DGS) to replace NeRF in their frameworks, significantly reducing the optimization time from several hours to dozens of minutes.

However, existing text-to-3D generation models face an inherent bottleneck in generation quality. Since the 3D priors are provided by the difference between rendered views and *pseudo ground truth* (pseudoGTs, i.e., the denoised images), the acquisition of “true” gradients requires a full denoising sampling, leading to considerable sampling costs for each iteration. To skip the full denoising sampling, Poole *et al.* and Liang *et al.* propose Score Distillation Sampling (SDS) and Interval Score Matching (ISM) objectives for swift generation, respectively. Despite SDS and ISM significantly reducing the optimization time, it comes at the cost of generation quality as their estimated gradients often deviate from the true ones. Specifically, to omit the terms of U-Net jacobians, SDS directly maps the noise to *pseudoGTs* using 1-step DDPM sampling, which leads to significant bias and produces over-smoothing contents. To address the over-smoothing issues, ISM first employs deterministic diffusing trajectories (i.e., DDIM inversion), and then simplifies the acquisition of true gradient into the interval scores at timestep t through omitting the weighted sum of interval scores *w.r.t* a series of timesteps. While ISM performs better than SDS in generation quality, this omission changes the magnitude and direction of the true gradients, which brings inconsistent updating direction to 3D models. Consequently, existing methods based on these objectives may lead to implausible and low-quality outcomes such as significant color deviation, frequently-occurred Janus problem, and semantically-inconsistent details (see Sec. IV-A and Fig. 2 in details).

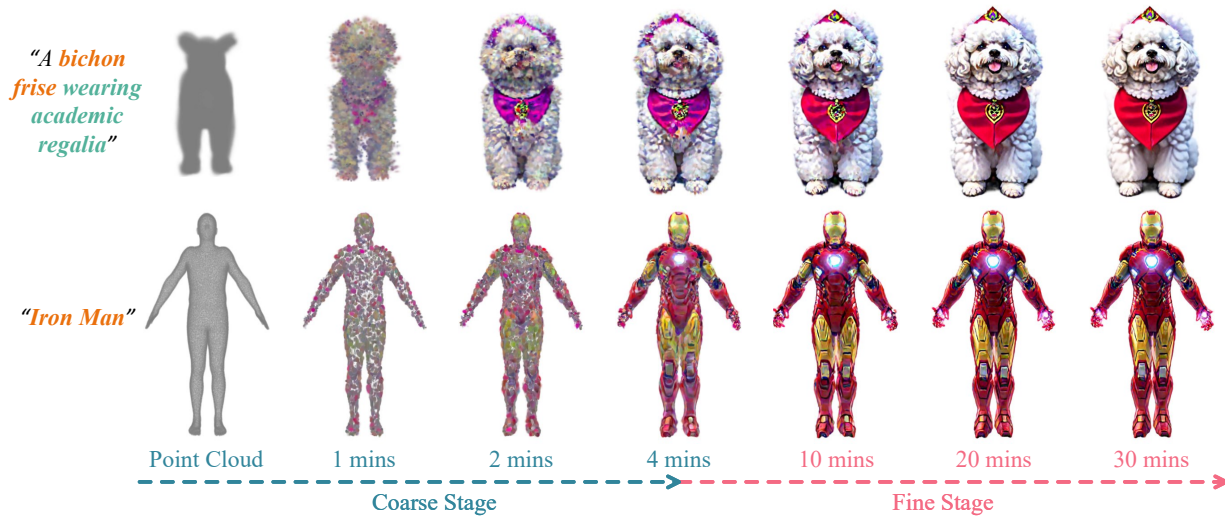
In this work, we propose *VividDreamer*, an efficient framework that can effectively address the inherent bottleneck of text-to-3D generation. Our key idea is to propose *Pose-dependent Consistency Distillation Sampling* (PCDS), a universal objective for diffusion-based 3D generation tasks. Inspired by Consistency Models [11], [12], our *PCDS* builds the *pose-dependent consistency function* within diffusion trajectories, enabling to skip the full denoising sampling and accurately estimate the gradients through 1~3 sampling steps. Specifically, *PCDS* first merges the pose-dependent scores based on Perp-Neg [13], and then maps the noise to *pseudoGTs* using consistency function in a classifier-free guidance (CFG) manner [14]. Compared with existing objectives, *PCDS* can acquire more accurate updating directions with the same sampling costs, while it further supports few-step (2~3) sampling

Manuscript received XXX XX, XXXX; revised XXX XX, XXXX. This work was supported in part by the National Natural Science Foundation of China under Grant 62072482. (Corresponding author: Xiaohua Xie.)

The authors are with the School of Computer Science and Engineering, Sun Yat-sen University, Guangzhou 510006, China; and with the Guangdong Province Key Laboratory of Information Security Technology, Guangzhou 510006, China; and also with the Key Laboratory of Machine Intelligence and Advanced Computing, Ministry of Education, Guangzhou 510006, China. (e-mail: {chenzx3, surj, zhujh59}@mail2.sysu.edu.cn; {yanglx9, stsjlh, xiexiaoh6}@mail.sysu.edu.cn)



(a) Text-to-3D Examples



(b) Training Process

Fig. 1. **Examples of text-to-3D asset creations with our framework** (a). We present an efficient text-to-3D generation framework – **VividDreamer** that can distill semantically-consistent textures and high-fidelity structures from pretrained 2D diffusion models using a novel **Pose-dependent Consistency Distillation Sampling** objective in a **coarse-to-fine optimization** manner, allowing to yield high-fidelity 3D objects (rows 1 and 2) and 3D avatars (row 3) based on the given text prompts. Specifically, our **VividDreamer** achieves high training efficiency, which can create ready-to-use 3D assets within 10 minutes, while producing photorealistic 3D objects within 30 minutes (b). More results can be found in Fig. 5 and our [Project page](#).

to trade compute for better generation quality. For an efficient generation, we tailor a coarse-to-fine optimization strategy to achieve a better balance between training time and generation quality, which first utilizes 1-step *PCDS* to create the basic structures, and then gradually increases *PCDS* steps to generate fine-grained details. We also introduce 3D Gaussian Splatting (3DGS) [15] to build our pipeline. As a result, *VividDreamer* achieves high training efficiency, enabling high-fidelity 3D object generation in a short time (see Fig. 1).

Extensive experiments demonstrate that *VividDreamer* favorably outperforms the state-of-the-art in generation quality,

effectively alleviating the implausible 3D generation issues caused by deviated updating direction in existing methods (see Fig. 4 in details). *VividDreamer* also achieves better training efficiency than the state-of-the-art, yielding higher generation quality with the same optimization time (see Fig. 6). *Notably*, only 10 minutes of training on a single A100 GPU achieves superior generation quality to the existing 3DGS-based methods, being favored by most users in the user study (see Table I).

Our framework has several other advantages: **i) High Consistency**. Thanks to the proposed *PCDS* that can counteract the semantic deviation brought by intrinsic randomness, our *Vivid-*

Dreamer enables to yield consistent *pseudoGTs* from various timesteps, significantly addressing the over-smoothing issues caused by SDS, producing more detailed results. Moreover, unlike ISM which is only applicable to DDIM sampling, our *PCDS* maintains such consistency in DDPM and DDIM sampling, **ii) High Adjustability**. Our *PCDS* enables various-step sampling to meet different speed-quality demands. **iii) High Versatility**. Our *PCDS* can be simply-applied into numerous 3D generative applications, creating high-quality 3D assets, please see Figs. 9 and 10 in details.

The main contributions are summarized as follows:

- We propose *VividDreamer*, a novel framework for high-fidelity and efficient text-to-3D generation.
- We propose Pose-dependent Consistency Distillation Sampling (PCDS) to address the inherent bottleneck in generation quality, and also tailor a coarse-to-fine optimization strategy for efficient 3D generation.
- Experiments on various 3D generation tasks show that *VividDreamer* favorably surpasses the state-of-the-art in generation quality and training efficiency.

The remainder of this paper is structured as follows. Related works and preliminaries are reviewed in Sections II and III, respectively. Section IV presents the analysis, motivation, and details of our approach. Section V demonstrates the experimental results and ablation study on text-to-3D generation. Section VI presents the results of other 3D generative applications. Conclusions and limitations are drawn in Section VII.

II. RELATED WORKS

A. Text-to-Image Diffusion Models

The field of text-to-image generation has experienced rapid development in recent years, largely thanks to advances in diffusion models [11], [16], [17] and CLIP [18]. Being trained on a rich text-to-image dataset such as [19], large diffusion models [2], [3], [20] are capable of generating impressive images consistent with a given text prompt conditioned on CLIP, becoming one of the core components for numerous currently-emerged generation and editing techniques. Beyond basic text-conditioning, diffusion models can be further conditioned by various modalities. One example is ControlNet [21], which can enhance the generation quality through the priors of depth or segmentation maps. However, diffusion generation is inherently slow as it relies on an iterative sampling process for denoising. This limits the development of downstream applications that require intensive queries, leading to massive training costs, especially in text-to-3D generation.

B. Differentiable 3D Representations

Creating a photorealistic 3D entity from discrete samples has been a long-standing research problem in the field of computer vision and graphics. One of the commonly used solutions is Neural Radiance Fields (NeRF) [1]. By utilizing standard volumetric rendering [22] and alpha compositing techniques [23], NeRF builds a differentiable rendering pipeline, yielding impressive novel view synthesis from conventional photos. A series of follow-up works extend NeRF [1] to the various

applications, such as generative 3D modeling [4], [24], 3D-editing [25], [26], surface reconstruction [27], and medical imaging [28]. Other methods aim to enhance NeRF on training efficiency and reconstruction quality, *e.g.*, few-view reconstruction [29], acceleration [30], and anti-aliasing [31]. Recently, 3D Gaussian Splatting (3DGS) [15] has become a hot method in this field, achieving remarkable training efficiency. In this paper, we introduce 3DGS to build the 3D rendering pipeline of our framework.

C. Text-to-3D Generation Models

With the breakthrough of key technologies in the fields of text-to-image generation and 3D representations, text-to-3D generation has become a reality. As a pioneer, DreamFusion [4] first extracts the 3D priors given by pre-trained 2D text-to-image diffusion models to generate 3D NeRF objects. Its core component is the Score Distillation Sampling (SDS), which facilitates 3D distillation by capturing the updating direction that conforms to text guidance, allowing for training a 3D model based on the 2D knowledge from diffusion models. Motivated by SDS, numerous follow-up works [5]–[10], [32]–[34] quickly sprout up to improve text-to-3D generation pipelines in various ways. Specifically, a group of methods [6]–[9] focus on better visual quality by modifying NeRF or introducing other efficient 3D representation techniques. Other improvements aim at seeking an optimal distribution [5] or solving the *Janus* problems [32]. Albeit promising, SDS has shown over-smoothing effects in many papers [4], [6], [33], while its improvements like Interval Score Matching (ISM) [10] generates semantically-inconsistent details (*e.g.*, color deviation), and others require a time-consuming sampling process [5], [34]. Our work is intrinsically different in the sense that it provides a theoretical analysis of the inconsistency and low-quality generation caused by SDS and ISM. We propose a universal approach Consistency Distillation Sampling (CDS), which can achieve superior generation quality with the same sampling costs as SDS and ISM, significantly addressing the above inherent bottleneck in text-to-3D generation.

III. PRELIMINARIES

A. Diffusion Models

Denoising Diffusion Probabilistic Model (DDPM). DDPM [16] assumes the inversion as a diffusion process according to a pre-defined schedule β_t on timestep t as:

$$p(x_t|x_{t-1}) = \mathcal{N}(x_t; \sqrt{1 - \beta_t}x_{t-1}, \beta_t I). \quad (1)$$

The posterior is modeled by a neural network ϕ as:

$$p_\phi(x_{t-1}|x_t) = \mathcal{N}(x_{t-1}; \sqrt{\bar{\alpha}_{t-1}}\mu_\phi(x_t), (1 - \bar{\alpha}_{t-1})\Sigma_\phi(x_t)), \quad (2)$$

where $\bar{\alpha}_t := (\prod_1^t(1 - \beta_t))$, while μ_ϕ and $\Sigma_\phi(x_t)$ denote the predicted mean and variance of x_t , respectively.

Denoising Diffusion Implicit Model (DDIM). Given an inversion trajectory $\{0, k, 2k, \dots, t - k, t\}$, DDIM [35] predicts invertible noisy latents as a deterministic diffusion trajectories:

$$x_t = \sqrt{\bar{\alpha}_t}\hat{x}_0^{t-k} + \sqrt{1 - \bar{\alpha}_t}\epsilon_\phi(x_{t-k}, t - k, \emptyset), \quad (3)$$

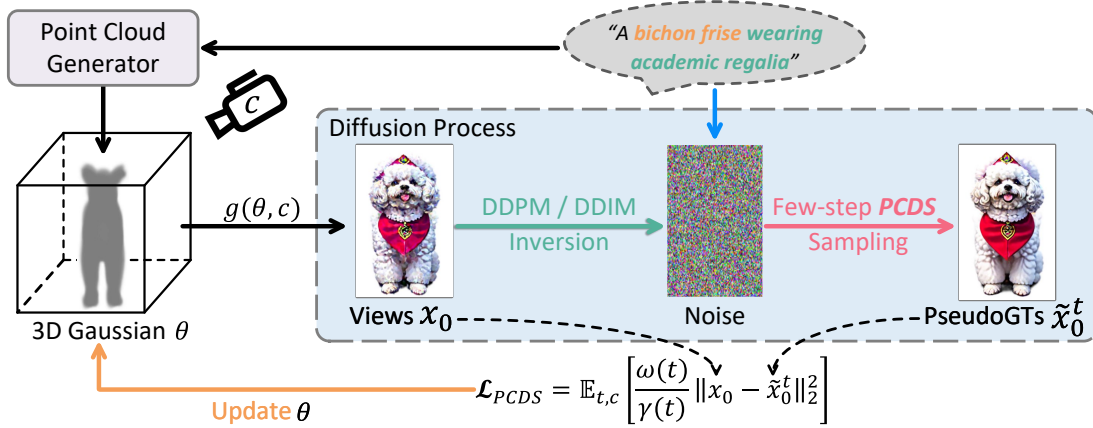


Fig. 2. An overview of *VividDreamer*. We employ 3D Gaussian Splatting (3DGS) [15] as 3D representation, and initialize it using the pre-trained Point-E [37] with given text prompts. In training, given a camera pose c , we render the corresponding view $x_0 = g(\theta, c)$ by the rendering pipeline of 3DGS, and disturb it to 2D diffusion models using DDPM/DDIM inversion. Then, we employ the proposed Pose-dependent Consistency Distillation Sampling (PCDS) to map noise x_t to the *pseudoGTs* \tilde{x}_0^t (i.e., the denoised images) through few-step (1~3) sampling. Finally, we calculate the Mean Square Error (MSE) loss \mathcal{L}_{PCDS} between the rendered views x_0 and *pseudoGTs* \tilde{x}_0^t , and update the parameter of 3D Gaussians θ by the gradients $\nabla_{\theta} \mathcal{L}_{PCDS}$ in Eq. (13).

where $\hat{x}_0^{t-k} = \frac{1}{\sqrt{\alpha_s}} x_{t-k} - \sqrt{1 - \alpha_t} \epsilon_{\phi}(x_{t-k}, t - k, \theta)$ denotes the *pseudoGTs* directly estimated from x_{t-k} using 1-step sampling. Thus, any point within that deterministic diffusion trajectory can be non-randomly estimated iteratively.

B. 3D Gaussian Splatting

3D Gaussian Splatting (3DGS) [15] is a recent groundbreaking method for novel view synthesis. Unlike NeRF [1] and its variants that render images based on volume rendering [22], 3DGS renders images through splatting [36], allowing extremely fast optimization and rendering speed. Specifically, 3DGS represents the scene through a set of 3D Gaussians. These 3D Gaussians can be defined with its center position $\mu \in \mathbb{R}^3$, covariance $\Sigma \in \mathbb{R}^7$, color $c \in \mathbb{R}^3$, and opacity $\alpha \in \mathbb{R}^1$, which can be queried as:

$$\mathcal{G}(p) = \exp\left(-\frac{1}{2}(p)^T \Sigma^{-1}(p)\right), \quad (4)$$

where p denotes the distance between μ and the query point. For computing the color of each pixel, 3DGS uses neural point-based rendering [36], i.e., simulating a ray r casting from the center of the camera to the end based on the corresponding camera pose c , which can be formulated as:

$$C(r) = \sum_{i \in \mathcal{N}} c_i \sigma_i \prod_{j=i}^{i-1} (1 - \sigma_j), \quad \sigma_i = \alpha_i \mathcal{G}(p_i), \quad (5)$$

where \mathcal{N} indicates the samples on the ray r , while σ_i , c_i , α_i and p_i denote the density, color, opacity, and distance of the i -th 3D Gaussians, respectively. Since the rendering process is differentiable, 3D Gaussians can be optimized using gradient descent. After optimization, 3DGS projects 3D Gaussians to 2D for rendering, yielding photorealistic novel views. Given a viewing transformation W , the covariance matrix Σ' in camera coordinates can be acquired as:

$$\Sigma' = JW \Sigma W^T J^T, \quad (6)$$

where J is the Jacobian of the affine approximation of the projective transformation.

IV. METHODS

In this section, we first analyze the limitations of Score Distillation Sampling (SDS) and Interval Score Matching (ISM) in text-to-3D generation. Subsequently, inspired by Consistency Models [11], [12] we propose Pose-dependent Consistency Distillation Sampling, a novel yet efficient objective that can acquire accurate gradients with minimal step sampling (1~3), significantly addressing the bottleneck of previous works in generation quality. Finally, we propose a two-stage framework for efficient text-to-3D generation, allowing high-fidelity 3D asset creation in a short training time. Figure 2 depicts the overall framework of our *VividDreamer*, and the subsequent techniques are described in the following subsections.

A. Review of SDS and ISM.

Given a 3D representation with learnable parameter θ , the differentiable rendering $x_0 = g(\theta, c)$ denotes to render 2D images x_0 based on the corresponding camera poses c . As shown in Fig. 3 (a), the true gradients can be calculated as:

$$\nabla_{\theta} \mathcal{L}_{true}(\theta) = \mathbb{E}_{t,c} \left[\frac{\omega(t)}{\gamma(t)} (x_0 - \tilde{x}_0^t) \frac{\partial g(\theta, c)}{\partial \theta} \right], \quad (7)$$

where $\omega(t)$ and $\gamma(t) = \frac{\sqrt{1 - \alpha_t}}{\sqrt{\alpha_t}}$ are the weight w.r.t different timesteps. \tilde{x}_0^t denotes the *pseudoGTs* obtained by full denoising sampling from the noise x_t to the timestep 0. Since the acquisition of \tilde{x}_0^t takes considerable sampling costs, SDS and ISM objectives aim to skip such a time-consuming process, which can be detailedly analyzed as follows:

Score Distillation Sampling (SDS). As shown in Fig. 2 (b), SDS objective can be formulated as:

$$\nabla_{\theta} \mathcal{L}_{SDS}(\theta) = \mathbb{E}_{t,c} \left[\frac{\omega(t)}{\gamma(t)} (x_0 - \hat{x}_0^t) \frac{\partial g(\theta, c)}{\partial \theta} \right], \quad (8)$$

where \hat{x}_0^t denotes the *pseudoGTs* directly estimated from the noise x_t using 1-step DDPM sampling based on Eq. (2). Due to the intrinsic randomness brought by DDPM, SDS faces two inherent limitations: *i*) inconsistent \hat{x}_0^t across different

timesteps t ; and *ii*) inaccurate 1-step estimation for all t , leading to blurred and sketchy results.

Interval Score Matching (ISM). Unlike SDS, Liang *et al.* non-randomly estimate x_t using DDIM inversion in Eq. (3), and thus Eq. (7) can be rewritten as:

$$\nabla_{\theta} \mathcal{L}_{true}(\theta) \triangleq \mathbb{E}_{t, \mathbf{c}} \left[\underbrace{(\omega(t) [\epsilon_{\phi}(x_t, t, y) - \epsilon_{\phi}(x_s, s, \theta)])}_{\text{interval score}} + \eta_t \frac{\partial g(\theta, \mathbf{c})}{\partial \theta} \right], \quad (9)$$

where $s = t - k$, and the bias term η_t is a weighted sum of interval scores *w.r.t* a series of timesteps. To skip full denoising sampling, ISM objective $\nabla_{\theta} \mathcal{L}_{ISM}$ directly omits the bias term η_t and only maintains the interval score at timestep t as:

$$\nabla_{\theta} \mathcal{L}_{ISM}(\theta) = \mathbb{E}_{t, \mathbf{c}} \left[(\omega(t) [\epsilon_{\phi}(x_t, t, y) - \epsilon_{\phi}(x_s, s, \theta)]) \frac{\partial g(\theta, \mathbf{c})}{\partial \theta} \right], \quad (10)$$

Since such omission changes the magnitude and direction of the true gradients $\nabla_{\theta} \mathcal{L}_{true}$, it leads to implausible outcomes, *e.g.*, color deviation, Janus problems, and semantically-inconsistent details in 3D models (see Figs. 4 and 7).

B. Pose-dependent Consistency Distillation Sampling

To mitigate the above problems exposed by SDS and ISM, we propose a novel sampling strategy dubbed Pose-dependent Consistency Distillation Sampling (PCDS) for text-to-3D generation. As analyzed in Sec. IV-A, the core problem of ISM is how to efficiently obtain consistent estimation \tilde{x}_0^t from any x_t . To this end, we only need to build a *consistency function* that can output consistent estimation \tilde{x}_0^t from any x_t on a certain trajectory with few-step (1 ~ 3) sampling (see Fig. 3 (c)). Inspired by [12], this function can be formally defined as $f_{\phi} : (x_t, t, y) \rightarrow \tilde{x}_0^t$, which can be further parameterized by:

$$f_{\phi} = f_{in}(t)x_0 + f_{out}(t)\mathcal{C}_{\phi}(x_t, t, y), \quad (11)$$

where f_{in} and f_{out} are differentiable functions with $f_{in}(0) = 1$ and $f_{out}(0) = 0$, and \mathcal{C}_{ϕ} is a neural network that outputs a tensor with the size of x_t . Concretely, we set $\mathcal{C}_{\phi}(x_t, t, y)$ as:

$$\mathcal{C}_{\phi}(x_t, t, y) = \frac{x_t}{\sqrt{\alpha_t}} - \gamma(t)\hat{\epsilon}_{\phi}(x_t, t, y), \quad t > 0, \quad (12)$$

which can be regarded as 1-step DDIM sampling [35]. Since \tilde{x}_0^t can be accurately estimated from x_t through few-step PCDS sampling, we can obtain an accurate and fast approximation of the true gradient $\nabla_{\theta} \mathcal{L}_{true}$ as:

$$\nabla_{\theta} \mathcal{L}_{PCDS}(\theta) \triangleq \mathbb{E}_{t, \mathbf{c}} \left[\frac{\omega(t)}{\gamma(t)} (x_0 - \tilde{x}_0^t) \frac{\partial g(\theta, \mathbf{c})}{\partial \theta} \right]. \quad (13)$$

Though classifier-free guidance (CFG) [14] has been widely used to construct $\hat{\epsilon}_{\phi}(x_t, t, y)$ in text-to-image generation, directly applying it to text-to-3D generation may bring about the notorious Janus problem, *e.g.*, yielding multi-faced objects. To further alleviate this problem, we incorporate pose-dependent prompts following Perp-Neg [13] into our PCDS. Specifically, given a camera pose \mathbf{c} , we generate its pose-dependent text

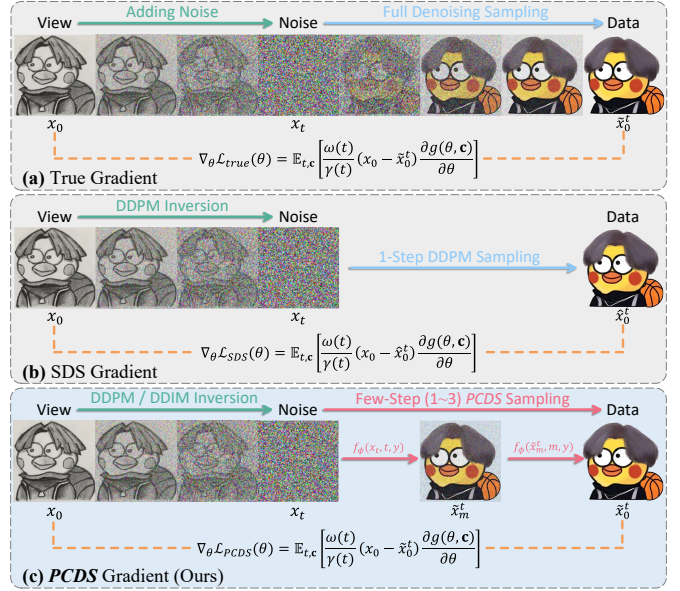


Fig. 3. Examples of different objectives. Visually, the acquisition of “true” gradient (a) is time-consuming work, requiring the full denoising sampling in each iteration. To skip such a lengthy process, Score Distillation Sampling (SDS) [4] (b) directly maps the noise to data *i.e.*, *pseudoGTs* using 1-step DDPM sampling, but SDS struggles to acquire accurate gradients due to the intrinsic randomness brought by DDPM. On the contrary, our PCDS builds the *pose-dependent consistency function* f_{ϕ} from any timestep t to the origin 0 within diffusion trajectories, allowing to generate accurate *pseudoGTs* and acquire precise gradients via minimal sampling steps (1~3).

embedding with the interpolation technique proposed in Perp-Neg. Then, we construct $\hat{\epsilon}_{\phi}(x_t, t, y)$ as follows:

$$\hat{\epsilon}_{\phi}(x_t, t, y) = \epsilon_{\phi}(x_t, t) + w_g \left[\epsilon_{\phi}^{pos} - \sum_{i=1}^{N_{neg}} w_c^{(i)} \epsilon_{\phi}^{neg^{(i)}} \right], \quad (14)$$

where N_{neg} denotes the number of negative prompts embeddings *w.r.t* camera pose \mathbf{c} , while w_g and $w_c^{(i)}$ indicate the weighting coefficients of positive and negative prompts embeddings, respectively. And ϵ_{ϕ}^{pos} and $\epsilon_{\phi}^{neg^{(i)}}$ are constructed from the unconditional term $\epsilon_{\phi}(x_t, t)$ as:

$$\begin{aligned} \epsilon_{\phi}^{pos} &= \epsilon_{\phi}(x_t, t, y_c^{pos}) - \epsilon_{\phi}(x_t, t), \\ \epsilon_{\phi}^{neg^{(i)}} &= \epsilon_{\phi}(x_t, t, y_c^{neg^{(i)}}) - \epsilon_{\phi}(x_t, t), \end{aligned} \quad (15)$$

where y_c^{pos} and $y_c^{neg^{(i)}}$ denote the positive and negative prompt embeddings *w.r.t* camera pose \mathbf{c} , respectively. Thus, the perpendicular gradient $\epsilon_{\phi}^{neg^{(i)}} \perp$ of $\epsilon_{\phi}^{neg^{(i)}}$ on ϵ_{ϕ}^{pos} can be estimated as:

$$\epsilon_{\phi}^{neg^{(i)}} \perp = \left(\epsilon_{\phi}^{neg^{(i)}} - \frac{\langle \epsilon_{\phi}^{pos}, \epsilon_{\phi}^{neg^{(i)}} \rangle}{\|\epsilon_{\phi}^{pos}\|^2} \epsilon_{\phi}^{pos} \right). \quad (16)$$

In practice, our PCDS first obtain the pose-dependent scores by Eq. (14), and then iteratively estimates the *pseudoGTs* in a CFG manner, which achieves robust sampling against Janus problem, enabling high-fidelity 3D object creation.

C. Coarse-to-Fine Optimization

As discussed, *PCDS* enables directly mapping the noise to *pseudoGTs* through 1-step sampling, while also allowing few-step (2~3) sampling to trade compute for higher generation quality. For efficient text-to-3D generation, we tailor a two-stage optimization strategy, which can generate 3D assets from coarse to fine, achieving high training efficiency. For clarity, we also provide pseudo codes in Algorithm 1.

In Coarse Stage, we aim to rapidly create an initial 3D structure from the given point cloud. For fast convergence, we first map the rendered views x_0 to noise x_t using DDPM inversion in Eq. (1), and then directly predict the *pseudoGTs* via a 1-step *PCDS* sampling. Thanks to the proposed *PCDS*, only 1-step sampling can acquire precise gradients for 3D object initialization, yielding better generation quality than SDS (see Fig. 7). The coarse stage only takes 4 minutes of training to create a nice structure from initial point clouds as shown in Fig. 1, effectively alleviating bizarre shapes caused by intrinsic randomness in the early training.

In Fine Stage, we aim to refine the 3D structures and generate fine-grained details. Specifically, to acquire more precise gradients, we utilize the DDIM inversion Eq. (3) instead of the DDPM inversion to non-randomly map the rendered views x_0 to noise x_t . We also gradually increase the sampling steps of *PCDS* from 1 to 3 with the increasing optimization steps, allowing the model to learn more fine-grained details from the diffusion-based 3D priors. As a result, *VividDreamer* can create ready-to-use 3D assets within 10 minutes, and producing photorealistic objects within 30 minutes (see Fig. 1).

D. Advanced Generation Pipeline

We also explore some factors that would affect the generation quality and propose an advanced pipeline with our *PCDS*. Specifically, we propose an efficient 3D representation technique and utilize ControlNet [21] for enhancement.

1) *Efficient Initialization*: Existing 3DGS-based methods usually adopt initial point cloud provided by text-to-point generative models [37], [38] for fast convergence. However, these text-to-point generative models cannot understand complex text prompts, usually yielding strange and irregular point clouds. Thus, the acquisition of the initial point cloud is a labor-consuming task because it requires manual conversion of text prompts into simple words, *e.g.*, converting ‘‘A hi-poly model of a yellow supercar’’ into ‘‘car’’. To address this issue, we utilize Chain-of-Thought (COT) [39] to teach the ChatGPT [40] how to extract simple prototypes from a complex text description. After training, ChatGPT can simplify a complex text description into one or two simple words. These words can be directly fed into the text-to-point generative models, obtaining point clouds with similar semantics, allowing to liberate researchers from heavy labor in manual conversions.

2) *ControlNet-based Enhancement*: Janus problem is a great challenge in text-to-3D generation tasks. Though our *PCDS* significantly alleviates the Janus problem caused by inaccurate gradients, it still cannot completely solve this problem because the text-to-image diffusion models do not truly understand the 3D objects in the real world. To achieve

ALGORITHM 1: Coarse-to-Fine Optimization

Input : Consistency model \mathcal{C}_ϕ , Coarse-stage iteration number N_c , Fine-stage iteration number N_f , DDIM inversion stepsize δ_t , and Target prompt embedding y .

```

for  $i \in \{0, 1, \dots, N_c + N_f - 1\}$  do
  if  $i < N_c$  then
    Sample:  $x_0 = g(\theta, c)$  and  $t \sim \mathcal{U}[600, 700]$ ;
    /* 1-step DDPM inversion */
     $x_t = \sqrt{\alpha_t}x_0 + \sqrt{1 - \alpha_t}\epsilon$ ,  $\epsilon \sim \mathcal{N}(\mathbf{0}, \mathbf{I})$ ;
     $\tilde{x}_0^t = \mathcal{C}_\phi(x_t, t, y)$ ; // 1-step PCDS sampling
  end
  else
    Sample:  $x_0 = g(\theta, c)$  and  $t \sim \mathcal{U}[300, 500]$ ;
    Initialize:  $x_t = x_0$ ;
    Let  $N_{inv} = \lceil t/\delta_t \rceil$ ;
    /* DDIM inversion in Eq. (3) */
    for  $j \in \{0, 1, \dots, N_{inv} - 1\}$  do
      Let  $t_f = \min(\lfloor (j+1)\delta_t \rfloor, t)$  and  $t_n = \lfloor j\delta_t \rfloor$ ;
       $\hat{x}_0^{t_n} = \frac{1}{\sqrt{\alpha_{t_n}}}(x_t - \sqrt{1 - \alpha_{t_n}}\epsilon_\phi(x_t, t_n, \emptyset))$ ;
       $x_t \leftarrow \sqrt{\alpha_{t_f}}\hat{x}_0^{t_n} + \sqrt{1 - \alpha_{t_f}}\epsilon_\phi(x_t, t_n, \emptyset)$ ;
    end
    Initialize:  $\tilde{x}_0^t = \mathcal{C}_\phi(x_t, t, y)$ ;
    Let  $N_p \in [1, 3]$  denote PCDS steps;
    /* Gradually increasing  $N_p$  */
    if  $N_p > 1$  then
      Let  $\delta_p = t/N_p$ ;
      for  $k \in \{N_p - 1, N_p - 2, \dots, 1\}$  do
        Let  $t_f = \lfloor k\delta_p \rfloor$  and  $t_n = \lfloor (k+1)\delta_p \rfloor$ ;
         $x_{t_f} = \sqrt{\alpha_{t_f}}\tilde{x}_0^t + \sqrt{1 - \alpha_{t_f}}\epsilon_\phi(x_{t_n}, t_n, y)$ ;
         $\tilde{x}_0^t \leftarrow \mathcal{C}_\phi(x_{t_f}, t_f, y)$ ;
      end
    end
  end
  Update  $\theta$  according to Eq. (13);
end

```

better 3D consistency, we optionally introduce ControlNet [21] to guide diffusion models, where the ControlNet priors are based on the depth maps related to the camera poses. This can successfully alleviate the Janus problem that appears in some specific text prompts, enabling better robustness against various situations.

V. EXPERIMENTS

In this section, we conduct extensive experiments and in-depth analysis to demonstrate the superiority of our *VividDreamer* in text-to-3D generation.

A. Implementation Details

In our framework, we adopt 3D Gaussian Splatting (3DGS) [15] as 3D representation and Stable Diffusion [2] finetuned by Latent Consistency Model [12] as diffusion-based 3D priors. We utilize the cloud point provided by the pre-trained Point-E [37] for initialization, and feed the camera-dependent prompts



Fig. 4. Visual comparisons between our framework and 4 state-of-the-art methods for text-to-3D generation. Experimental results show that our approach is capable of creating high-fidelity 3D assets that maintain consistent semantics with the given text prompts, significantly alleviating the color deviation, Janus problem, and semantically inconsistent details caused by inaccurate gradient estimation. The training time is evaluated on a single A100 GPU.

suggested in Perp-Neg [13] into diffusion models. To further alleviate the Janus problem using ControlNet [21], we first render the depth maps related to the camera poses using 3DGS, and then feed these rendered depth maps into ControlNet to guide the generation of diffusion models. The batch size is set to 4, and the iteration numbers of coarse stage N_c and fine stage N_f are set to 500 and 2500, respectively. The DDIM inversion stepsize δ_t is fixed as 200, and the iteration numbers of 1-, 2-, and 3-step PCDS sampling are set to 1000, 800, and 700, respectively. *Note*, we can acquire ready-to-use 3D assets within 10 minutes (nearly 1500 iterations), and obtaining high-fidelity objects within 30 minutes (3000 iterations).

B. Comparison Results

We primarily compare with four baselines, including DreamFusion [4], DreamGaussian [9], GaussianDreamer [9] and LucidDreamer [10], where DreamFusion is re-implemented by [41] using NGP [30] and Stable Diffusion [2], and the rest methods are built by 3DGS and Stable Diffusion.

1) *Qualitative Comparisons*: We provide qualitative comparisons on text-to-3D generation in Fig. 4. As shown, our *VividDreamer* outperforms the competitors especially *w.r.t* high-quality visual appearance, significantly alleviating the color deviation caused by inaccurate gradients. We also found that directly using Perp-Neg [13] can only alleviate the Janus problem that appears in some text prompts. For example,

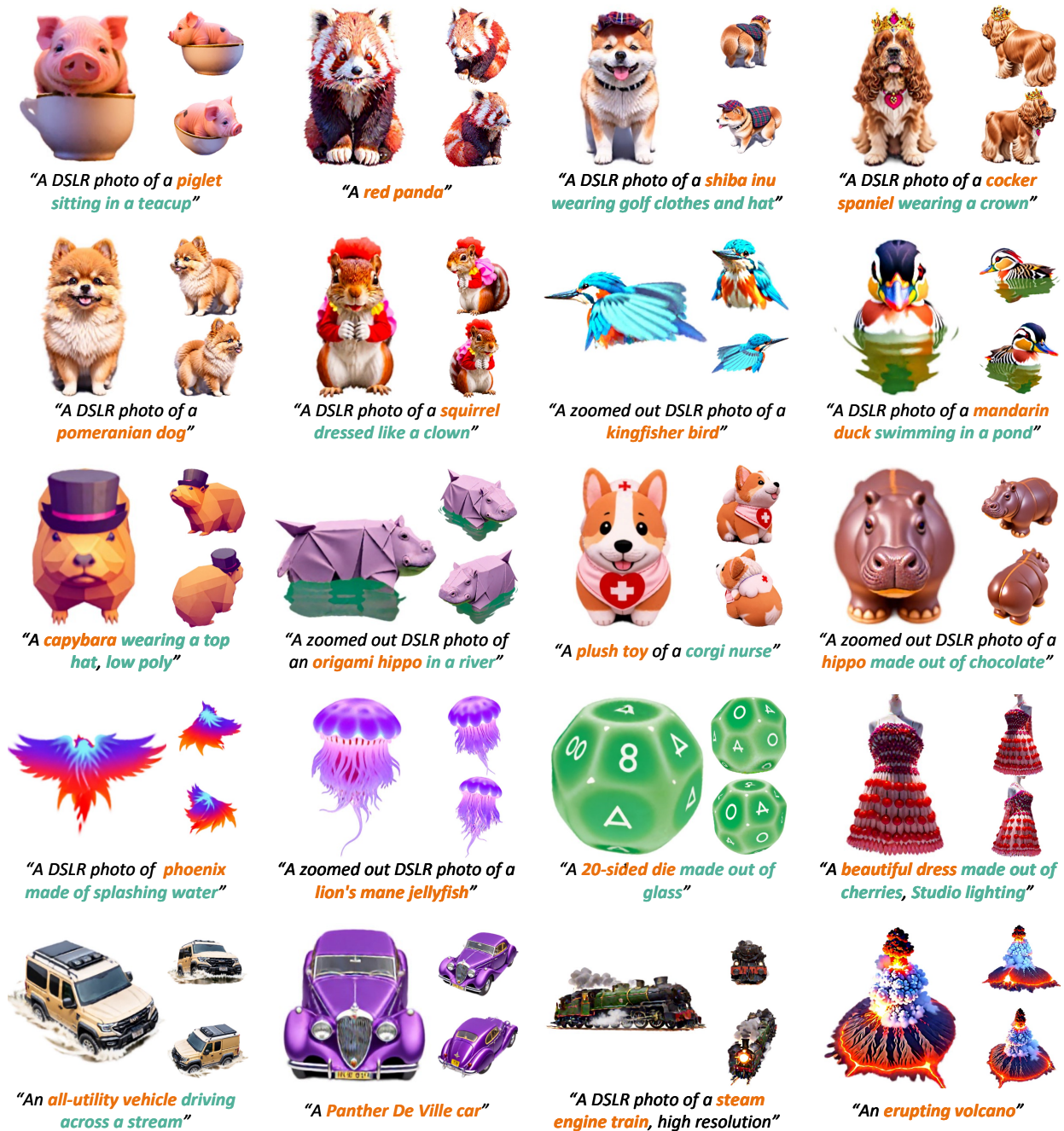


Fig. 5. Visual results generated by our *VividDreamer* framework with 30 minutes of training on a single A100 GPU. As shown, our approach creates high-fidelity 3D assets based on various text prompts. More visual results can be found in our [Project page](#).

though GaussianDreamer [9] and LucidDreamer [10] incorporate Perp-Neg into their 3D generation pipeline, they still produce multi-faceted and 3D-inconsistent objects. Thanks to *PCDS* that neatly combines Perp-Neg into the built-in consistency function, *VividDreamer* can effectively alleviate the Janus problem brought by inaccurate gradients and the intrinsic limitation of text-to-image diffusion models, yielding lifelike 3D assets with high-fidelity geometric structures. Moreover, *VividDreamer* generates semantically consistent results, faithfully restoring the details overlooked by the compared methods. We also provide more visual results in Fig. 5, and more visual comparisons can be found in our [Project page](#).

To better exhibit our training efficiency, we further compare the results against baselines under a 10-minute training. As shown in Fig. 6, LucidDreamer [10] falls short in good convergence within 10 minutes of training, yielding sub-optimal results. While GaussianDreamer [9] can be well-converged in 10 minutes, it is limited by the inaccurate gradient estimation from SDS, producing low-quality 3D objects. On the contrary, *VividDreamer* achieves superior generation quality with the same optimization time, presenting a noteworthy training efficiency. It also demonstrates that *VividDreamer* significantly addresses the bottleneck in existing text-to-3d generation methods, proving the correctness and effectiveness



Fig. 6. Visual comparisons between our *VividDreamer* and 2 state-of-the-art methods: *LucidDreamer* [10], and *GaussianDreamer* [9] for text-to-3D generation, where the results are generated by ~ 10 minutes of training on a single A100 GPU. Visually, our framework enables high-fidelity 3D object creations within a such short time, presenting a noteworthy training efficiency.

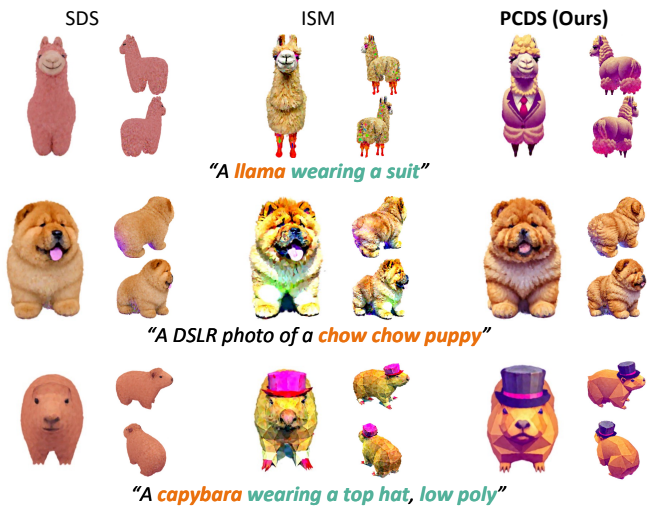


Fig. 7. Visual comparisons between our Pose-dependent Consistency Distillation Sampling *PCDS* and 2 existing objectives: Score Distillation Sampling (SDS) [4] and Interval Score Matching (ISM) [10]. The results are generated by incorporating these objectives into our framework with a 30-minute training without any modifications and extra processing.

of our motivation and model design.

2) *User Study*: We conduct a user study to provide a comprehensive evaluation of text-to-3D generation quality. Specifically, we randomly select 50 prompts from a total of 414 ones for evaluation, and generate 3D objects using 5 different methods (including our 10- and 30-minute versions) with each prompt. For fair comparisons, we anonymize all the methods, and exhibit each 3D asset by its 360° rendered video. Users are invited to fill out the questionnaire online, and asked to rank the 3D objects based on the fidelity and the degree of alignment with the given text prompt. Table I reports the results summarized from 98 questionnaires on the internet, where we evaluate users’ preferences using the average ranking. As shown, our *VividDreamer* achieves the

TABLE I

WE SURVEY THE AVERAGE RANKING OF USERS’ PREFERENCE ON 50 SETS OF TEXT-TO-3D GENERATION RESULTS PRODUCED BY THE STATE-OF-THE-ART AND OUR 10- AND 30-MINUTE VERSIONS, RESPECTIVELY. OUR RESULTS ARE PREFERRED BY MOST USERS. THE TRAINING TIME IS EVALUATED ON A SINGLE A100 GPU.

Methods	Avg. Rank ↓	Training Time ↓
DreamGaussian [8]	4.74	3 mins
GaussianDreamer [9]	3.41	9 mins
LucidDreamer [10]	2.65	45 mins
VividDreamer₁₀ (Ours)	2.26	10 mins
VividDreamer₃₀ (Ours)	1.43	30 mins

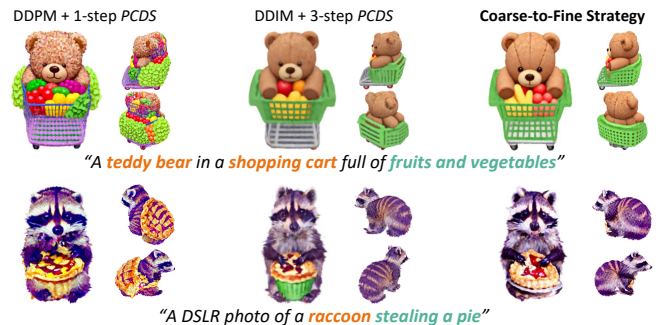


Fig. 8. Visual comparisons between different ablations of our framework. The results are generated under 10 minutes of training on a single A100 GPU. Visually, the proposed coarse-to-fine optimization strategy acquires superior generation quality to the competitors in the same training time, achieving better training efficiency.

highest average ranking, demonstrating that users consistently favored the 3D objects generated by our framework. This also demonstrates that *VividDreamer* achieves a high training efficiency, only 10 minutes of training on a single A100 GPU can outperform the competitors.

C. Ablation Study

In this subsection, we carry out ablation studies to investigate the effectiveness of the proposed modules.

1) *Different Objectives*: We evaluate the visual quality of our framework based on different objectives: SDS, ISM, and our *PCDS*. Specifically, for each objective, we incorporate it into our framework and conduct training of 3000 iterations. All the hyperparameters and model settings are consistent. During training, we gradually increase the sampling steps of our *PCDS* from 1 to 3. As shown in Fig. 7, *PCDS* achieves better generation quality than SDS and ISM, producing high-fidelity and semantically-inconsistent 3D assets. This also proves that our *PCDS* can alleviate the color deviation and Janus problem caused by the inaccurate gradient estimation.

2) *Different Optimization Strategies*: In Fig. 8, we evaluate the training efficiency of the following optimization strategies: *only 1-step PCDS*, *only 3-step PCDS*, and our *coarse-to-fine strategy*, *i.e.*, gradually increasing the sampling steps of *PCDS* from 1 to 3. With the same training time (10 minutes), our *coarse-to-fine* results achieve higher generation quality, producing 3D-consistent structures and finer details, which proves the effectiveness of our designs.



Fig. 9. Visual examples of 3D portraits and avatars. As shown, our approach can create high-quality 3D avatars and portraits within 30 minutes of training on a single A100 GPU.

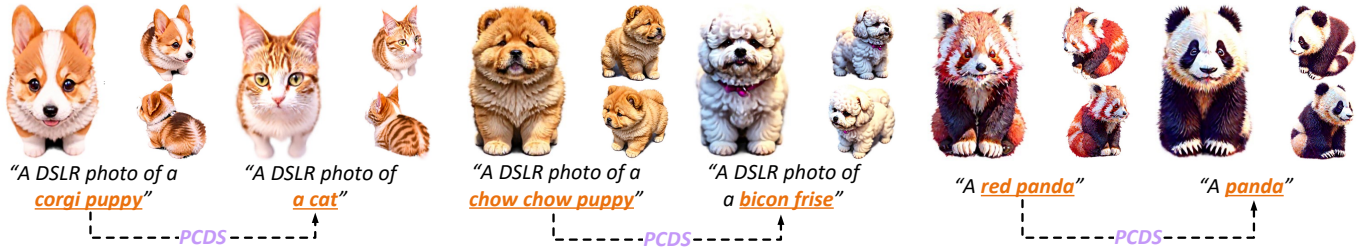


Fig. 10. Visual examples of editing the given 3D assets with user-guided prompts using the proposed PCDS. As shown, our approach can create user-desired 3D objects while maintaining the basic structure of the prototypes.

VI. APPLICATIONS

In this section, we further explore the effectiveness of our work on other 3D generative applications, such as zero-shot 3D avater and portrait generation, and zero-shot 3D editing.

A. Zero-shot 3D Avatar & Portrait Generation

We expand our *VividDreamer* to generate 3D avatars and portraits from text descriptions. To generate 3D avatars, we utilize the Skinned Multi-Person Linear Model (SMPL) [42] to generate the point cloud of the human body as a geometry prior to 3DGS initialization. We also employ ControlNet [21] conditioned on depth maps to offer more robust supervision during training. For 3D portrait creation, 3DGS is initialized by the point cloud of “head” provided from Point-E [37]. As shown in Fig. 9, only following such a simple process, *VividDreamer* can generate high-fidelity 3D avatars (row 1) and portraits (rows 2 and 3) that consistent with text prompts.

B. Zero-shot 3D Editing

In addition to text-to-3D generation tasks, our *PCDS* can also be simply extended to 3D editing tasks. Because *PCDS* can acquire updating direction that consistent with text prompts, it enables editing the textures of an arbitrary 3D asset based on a user-guided text prompt in a zero-shot manner.

Specifically, given a 3D asset and a text prompt, we first transform the 3D asset into a point cloud to initialize 3DGS. Then, we employ the depth map-prior ControlNet [21] to guide the optimization. As shown in Fig. 10, the edited results show high-quality details consistent with the given text prompts, while maintaining the basic structure of original 3D objects.

VII. CONCLUSIONS

In this work, we present *VividDreamer*, a text-to-3D generation framework that significantly improves the efficiency of 3D content creation. We design an efficient Pose-dependent Consistency Distillation Sampling (PCDS) objective, and propose a coarse-to-fine optimization framework, enabling high-fidelity 3D object creation in a short time. Thanks to the proposed modules, our approach can first create ready-to-use 3D assets within 10 minutes, and then produce high-fidelity 3D structures and fine-grained details within 30 minutes. Extensive experiments demonstrate that our *VividDreamer* favorably outperforms the state-of-the-art in generation quality and training efficiency. Its outstanding performance paves the way for a wide range of 3D generative applications, such as text-to-3D editing and zero-shot avatar creation, making it possible to facilitate numerous applications in the real world.

REFERENCES

- [1] B. Mildenhall, P. P. Srinivasan, M. Tancik, J. T. Barron, R. Ramamoorthi, and R. Ng, "Nerf: Representing scenes as neural radiance fields for view synthesis," *Commun. ACM*, vol. 65, no. 1, pp. 99–106, 2021. **1, 3, 4**
- [2] R. Rombach, A. Blattmann, D. Lorenz, P. Esser, and B. Ommer, "High-resolution image synthesis with latent diffusion models," in *IEEE Conf. Comput. Vis. Pattern Recog.*, June 2022, pp. 10 684–10 695. **1, 3, 6, 7**
- [3] C. Saharia, W. Chan, S. Saxena, L. Li, J. Whang, E. L. Denton, K. Ghasemipour, R. Gontijo Lopes, B. Karagol Ayan, T. Salimans *et al.*, "Photorealistic text-to-image diffusion models with deep language understanding," *Adv. Neural Inform. Process. Syst.*, vol. 35, pp. 36 479–36 494, 2022. **1, 3**
- [4] B. Poole, A. Jain, J. T. Barron, and B. Mildenhall, "Dreamfusion: Text-to-3d using 2d diffusion," in *Int. Conf. Learn. Represent.*, 2022. **1, 3, 5, 7, 9**
- [5] Z. Wang, C. Lu, Y. Wang, F. Bao, C. Li, H. Su, and J. Zhu, "Prolificdreamer: High-fidelity and diverse text-to-3d generation with variational score distillation," in *Adv. Neural Inform. Process. Syst.*, 2023. **1, 3**
- [6] C.-H. Lin, J. Gao, L. Tang, T. Takikawa, X. Zeng, X. Huang, K. Kreis, S. Fidler, M.-Y. Liu, and T.-Y. Lin, "Magic3d: High-resolution text-to-3d content creation," in *IEEE Conf. Comput. Vis. Pattern Recog.*, 2023, pp. 300–309. **1, 3**
- [7] R. Chen, Y. Chen, N. Jiao, and K. Jia, "Fantasia3d: Disentangling geometry and appearance for high-quality text-to-3d content creation," in *Int. Conf. Comput. Vis.*, 2023, pp. 22 246–22 256. **1, 3**
- [8] J. Tang, J. Ren, H. Zhou, Z. Liu, and G. Zeng, "Dreamgaussian: Generative gaussian splatting for efficient 3d content creation," in *Int. Conf. Learn. Represent.*, 2023. **1, 3, 9**
- [9] T. Yi, J. Fang, J. Wang, G. Wu, L. Xie, X. Zhang, W. Liu, Q. Tian, and X. Wang, "Gaussiandreamer: Fast generation from text to 3d gaussians by bridging 2d and 3d diffusion models," in *IEEE Conf. Comput. Vis. Pattern Recog.*, 2024. **1, 3, 7, 8, 9**
- [10] Y. Liang, X. Yang, J. Lin, H. Li, X. Xu, and Y. Chen, "Luciddreamer: Towards high-fidelity text-to-3d generation via interval score matching," in *IEEE Conf. Comput. Vis. Pattern Recog.*, 2024. **1, 3, 7, 8, 9**
- [11] Y. Song, P. Dhariwal, M. Chen, and I. Sutskever, "Consistency models," in *Int. Conf. Learn. Represent.*, 2023, pp. 32 211–32 252. **1, 3, 4**
- [12] S. Luo, Y. Tan, L. Huang, J. Li, and H. Zhao, "Latent consistency models: Synthesizing high-resolution images with few-step inference," *arXiv preprint arXiv:2310.04378*, 2023. **1, 4, 5, 6**
- [13] M. Armandpour, A. Sadeghian, H. Zheng, A. Sadeghian, and M. Zhou, "Re-imagine the negative prompt algorithm: Transform 2d diffusion into 3d, alleviate janus problem and beyond," *arXiv preprint arXiv:2304.04968*, 2023. **1, 5, 7**
- [14] J. Ho and T. Salimans, "Classifier-free diffusion guidance," in *NeurIPS Workshop on Deep Generative Models and Downstream Applications*, 2021. **1, 5**
- [15] B. Kerbl, G. Kopanas, T. Leimkühler, and G. Drettakis, "3d gaussian splatting for real-time radiance field rendering," *ACM Trans. Graph.*, vol. 42, no. 4, pp. 1–14, 2023. **2, 3, 4, 6**
- [16] J. Ho, A. Jain, and P. Abbeel, "Denosing diffusion probabilistic models," *Adv. Neural Inform. Process. Syst.*, vol. 33, pp. 6840–6851, 2020. **3**
- [17] Y. Song, J. Sohl-Dickstein, D. P. Kingma, A. Kumar, S. Ermon, and B. Poole, "Score-based generative modeling through stochastic differential equations," in *Int. Conf. Learn. Represent.*, 2020. **3**
- [18] A. Radford, J. W. Kim, C. Hallacy, A. Ramesh, G. Goh, S. Agarwal, G. Sastry, A. Askell, P. Mishkin, J. Clark *et al.*, "Learning transferable visual models from natural language supervision," in *Int. Conf. Mach. Learn.* PMLR, 2021, pp. 8748–8763. **3**
- [19] C. Schuhmann, R. Beaumont, R. Vencu, C. Gordon, R. Wightman, M. Cherti, T. Coombes, A. Katta, C. Mullis, M. Wortsman *et al.*, "Laion-5b: An open large-scale dataset for training next generation image-text models," *Adv. Neural Inform. Process. Syst.*, vol. 35, pp. 25 278–25 294, 2022. **3**
- [20] A. Q. Nichol, P. Dhariwal, A. Ramesh, P. Shyam, P. Mishkin, B. McGrew, I. Sutskever, and M. Chen, "GLIDE: Towards photorealistic image generation and editing with text-guided diffusion models," in *Int. Conf. Mach. Learn.*, ser. Proceedings of Machine Learning Research, vol. 162. PMLR, 17–23 Jul 2022, pp. 16 784–16 804. **3**
- [21] L. Zhang, A. Rao, and M. Agrawal, "Adding conditional control to text-to-image diffusion models," in *Int. Conf. Comput. Vis.*, 2023, pp. 3836–3847. **3, 6, 7, 10**
- [22] J. T. Kajiya and B. P. Von Herzen, "Ray tracing volume densities," *ACM SIGGRAPH computer graphics*, vol. 18, no. 3, pp. 165–174, 1984. **3, 4**
- [23] T. Porter and T. Duff, "Compositing digital images," in *Proceedings of the 11th annual conference on Computer graphics and interactive techniques*, 1984, pp. 253–259. **3**
- [24] K. Schwarz, Y. Liao, M. Niemeyer, and A. Geiger, "Graf: Generative radiance fields for 3d-aware image synthesis," *Adv. Neural Inform. Process. Syst.*, vol. 33, pp. 20 154–20 166, 2020. **3**
- [25] Y.-J. Yuan, Y.-T. Sun, Y.-K. Lai, Y. Ma, R. Jia, and L. Gao, "Nerf-editing: geometry editing of neural radiance fields," in *IEEE Conf. Comput. Vis. Pattern Recog.*, 2022, pp. 18 353–18 364. **3**
- [26] C. Bao, Y. Zhang, B. Yang, T. Fan, Z. Yang, H. Bao, G. Zhang, and Z. Cui, "Sine: Semantic-driven nerf editing with prior-guided editing field," in *IEEE Conf. Comput. Vis. Pattern Recog.*, 2023. **3**
- [27] P. Wang, L. Liu, Y. Liu, C. Theobalt, T. Komura, and W. Wang, "Neus: Learning neural implicit surfaces by volume rendering for multi-view reconstruction," in *Adv. Neural Inform. Process. Syst.*, 2021. **3**
- [28] Z. Chen, J. Lai, L. Yang, and X. Xie, "Cunerf: Cube-based neural radiance field for zero-shot medical image arbitrary-scale super resolution," 2023. **3**
- [29] A. Yu, V. Ye, M. Tancik, and A. Kanazawa, "pixelnerf: Neural radiance fields from one or few images," in *IEEE Conf. Comput. Vis. Pattern Recog.*, 2021, pp. 4578–4587. **3**
- [30] T. Müller, A. Evans, C. Schied, and A. Keller, "Instant neural graphics primitives with a multiresolution hash encoding," *ACM Trans. Graph.*, vol. 41, no. 4, pp. 1–15, 2022. **3, 7**
- [31] J. T. Barron, B. Mildenhall, M. Tancik, P. Hedman, R. Martin-Brualla, and P. P. Srinivasan, "Mip-nerf: A multiscale representation for anti-aliasing neural radiance fields," 2021. **3**
- [32] Y. Shi, P. Wang, J. Ye, L. Mai, K. Li, and X. Yang, "Mvdream: Multi-view diffusion for 3d generation," in *Int. Conf. Learn. Represent.*, 2023. **3**
- [33] E. Richardson, G. Metzger, Y. Alaluf, R. Giryes, and D. Cohen-Or, "Texture: Text-guided texturing of 3d shapes," in *ACM SIGGRAPH Conference Proceedings*, 2023, pp. 1–11. **3**
- [34] J. Zhu and P. Zhuang, "Hifa: High-fidelity text-to-3d with advanced diffusion guidance," *arXiv preprint arXiv:2305.18766*, 2023. **3**
- [35] J. Song, C. Meng, and S. Ermon, "Denosing diffusion implicit models," in *International Conference on Learning Representations*, 2020. **3, 5**
- [36] G. Kopanas, J. Philip, T. Leimkühler, and G. Drettakis, "Point-based neural rendering with per-view optimization," in *Computer Graphics Forum*, vol. 40, no. 4, 2021. **4**
- [37] A. Nichol, H. Jun, P. Dhariwal, P. Mishkin, and M. Chen, "Point-e: A system for generating 3d point clouds from complex prompts," *arXiv preprint arXiv:2212.08751*, 2022. **4, 6, 10**
- [38] H. Jun and A. Nichol, "Shap-e: Generating conditional 3d implicit functions," *arXiv preprint arXiv:2305.02463*, 2023. **6**
- [39] J. Wei, X. Wang, D. Schuurmans, M. Bosma, F. Xia, E. Chi, Q. V. Le, D. Zhou *et al.*, "Chain-of-thought prompting elicits reasoning in large language models," *Adv. Neural Inform. Process. Syst.*, vol. 35, pp. 24 824–24 837, 2022. **6**
- [40] OpenAI, "Chatgpt (version 3.5)," 2021. [Online]. Available: <https://chat.openai.com> **6**
- [41] J. Tang, "Stable-dreamfusion: Text-to-3d with stable-diffusion," 2022, <https://github.com/ashawkey/stable-dreamfusion>. **7**
- [42] M. Loper, N. Mahmood, J. Romero, G. Pons-Moll, and M. J. Black, "Smpl: a skinned multi-person linear model," *ACM Trans. Graph.*, vol. 34, no. 6, oct 2015. **10**